



# Resolving electrochemically triggered topological defect dynamics and structural degradation in layered oxides

Chunyang Wang<sup>a,b,1,2</sup> , Rui Zhang<sup>a,1</sup>, Ju Li<sup>c,d,2</sup> , and Huolin L. Xin<sup>a,2</sup>

Affiliations are included on p. 6.

Edited by Yi Cui, Stanford University, Stanford, CA; received May 19, 2024; accepted November 20, 2024

Understanding topological defects-controlled structural degradation of layered oxides—a key cathode material for high-performance lithium-ion batteries—plays a critical role in developing next-generation cathode materials. Here, by constructing a nanobattery in an electron microscope enabling atomic-scale monitoring of electrochemical reactions, we captured the electrochemically driven atomistic dynamics and evolution of dislocations—a most important topological defect in material. We deciphered how dislocations nucleate, move, and annihilate within layered cathodes at the atomic scale. Specifically, we found two types of dislocation configurations, i.e., single dislocations and dislocation dipoles. Both pure dislocation glide/climb and mixed motions were captured, and the dislocation glide and climb velocities were first experimentally measured. Moreover, dislocation activity-mediated structural degradation such as crack nucleation, phase transformation, and lattice reorientation was unraveled. Our work provides deep insights into the atomistic dynamics of electrochemically driven dislocation activities in layered oxides.

layered oxide | cathode | lithium-ion batteries | defect | dislocation

Dislocation, as one of the most important topological defects (1), widely exists in ductile metals and is the main carrier of their plastic deformation (2–4). Yet, for inherently brittle ceramic materials, dislocations are not common (5). In fact, for a long time, materials scientists have considered that in oxide ceramics, plastic deformation by dislocation motion does not occur at low homologous temperatures or occurs to such a limited extent that cracks are sharp to the atomic level (6). Different from the scenario that dislocations in structural ceramics (if they are not nonexistent) could only be triggered by pure mechanical loading (7), the formation of dislocations in functional ceramics could be induced by versatile external stimuli such as electric field, temperature field, and electrochemical driving force (external mechanical stress could also be involved). Among all external fields that trigger topological defects, the electrochemical driving force is special because the local valence states and stoichiometry of ceramics are constantly altered and rapidly evolving during nonequilibrium electrochemical processes (8). Therefore, the atomic-scale defects generation and evolution dynamics in ceramics driven by the electrochemical process could be extremely complex (9, 10). However, so far, due to the spatial resolution limit of optical microscopy, X-ray-based techniques as well as the temporal resolution limitation of current ex-situ transmission electron microscopy, it remains a grand challenge to directly visualize the dynamic behaviors of electrochemically driven topological defects under operating conditions, in real-time, and at the atomic scale.

Layered oxides are a class of technologically important ceramics widely used as cathodes for lithium-ion batteries (11–18). During electrochemical charge–discharge process, lithium ions were repeatedly extracted and reinserted into the lattice of layered ceramics, during which considerable inhomogeneous lattice strain accumulates, thus resulting in the formation of multiple nanoscale phase domains (e.g., H2, H3 phases) in single particles. Generally, with lithium ions deintercalated from the oxide, its *c* axis first expands and then significantly shrinks (19). The expansion is usually attributed to the formation of the H2 phase, while the shrinkage is attributed to the H3 phase (20, 21) or, more notably, the detrimental O1 phase, which has recently garnered significant attention in high-Ni cathodes following its first atomic-scale identification (22–24). Due to lattice nonuniformity induced by inhomogeneous Li-ion diffusion at the nano- and atomic-scale, topological defects such as dislocations incline to form between domains of different electrochemical states. These misfit dislocations, which accommodate the transformation strain between inhomogeneously delithiated domains, are different from dislocations in a uniform single-phase crystal. The misfit dislocation could also significantly influence lithium-ion transport at the domain/phase boundary and thereby the performance of the

## Significance

Topological defects play a critical role in the degradation of layered oxide—an important cathode material for lithium-ion batteries, yet, to date, an atomic-scale understanding of these topological defects and their behaviors/influences still remains a mystery. Here, by employing an in situ transmission electron microscopy (TEM) technique, we deciphered how dislocations nucleate, move, and annihilate at the atomic scale during electrochemical reaction in an archetypal layered oxide cathode. The dislocation glide and climb velocities were experimentally measured. Equally importantly, dislocation activity-mediated structural degradation such as crack nucleation, phase transformation, and lattice reorientation was unraveled. Our work, by resolving the atomistic dynamics of electrochemically driven dislocation activities, offers deep insights into the topological defects-controlled structural evolution/degradation of layered oxides.

Author contributions: C.W., J.L., and H.L.X. designed research; C.W. and R.Z. performed research; C.W. analyzed data; and C.W. wrote the paper with help from all authors.

The authors declare no competing interest.

This article is a PNAS Direct Submission.

Copyright © 2025 the Author(s). Published by PNAS. This article is distributed under [Creative Commons Attribution-NonCommercial-NoDerivatives License 4.0 \(CC BY-NC-ND\)](https://creativecommons.org/licenses/by-nc-nd/4.0/).

<sup>1</sup>C.W. and R.Z. contributed equally to this work.

<sup>2</sup>To whom correspondence may be addressed. Email: wangchunyang@imr.ac.cn, liju@mit.edu, or huolin.xin@uci.edu.

This article contains supporting information online at <https://www.pnas.org/lookup/suppl/doi:10.1073/pnas.2409494122/-/DCSupplemental>.

Published January 13, 2025.

electrodes. So far, a fundamental understanding of how the misfit dislocations nucleate, move, and interact under nonuniform electrochemical conditions is a mystery. In this work, using operando atomic-resolution electron microscopy, we systematically investigate the dislocation activities in an archetypal layered oxide cathode driven by nonuniform ion deintercalation. Our work, by deciphering the dislocation activities driven by atomic-scale non-uniform ion transport, shed important insights into the behaviors of topological defects in layered oxides.

## Results

To in situ track the structural evolution of the layered oxides during Li-ion deintercalation, lithium nickelate particles (see detailed characterization in *SI Appendix, Figs. S1–S3*) were inserted between two electrodes with which a voltage can be applied to the object of interest to initiate delithiation (25, 26) (see experimental setup and an evaluation of beam effects in *SI Appendix, Figs. S4 and S5* and *Materials and Methods*). Fig. 1 *A* and *B* and *SI Appendix, Figs. S6 and S7* show representative high-resolution transmission electron microscopy (HRTEM) images and corresponding strain maps of lithium nickelate after Li-ion deintercalation in TEM at  $\sim 5$  V. We found that substantial misfit edge dislocations (inset shows an edge dislocation with the extra half-plane highlighted, see detailed analysis of the edge nature of the dislocation in *SI Appendix, Fig. S8*) formed in the delithiated lattice. Interestingly, the randomly distributed dislocations can be classified into two types, i.e., single dislocations and dislocation dipoles (composed of two dislocations of opposite signs) (Fig. 1*B*). Fig. 1*C* shows a representative atomic-resolution high-angle annular dark-field scanning TEM (HAADF-STEM) image and corresponding strain maps of lithium nickelate electrochemically charged to 4.4 V in coin-cell batteries. Misfit single dislocations and dislocation dipoles

similar to that formed in situ in TEM (Fig. 1*B*) were also identified, indicating the in situ method is basically equivalent to coin-cell electrochemical operations in terms of ion deintercalation.

Next, the moving velocities of these dislocations were monitored as a function of delithiation time (*Movie S1*). By in situ tracking the trajectories of dislocation cores, the velocities of these misfit dislocations were quantitatively measured. Note that, HRTEM imaging (27) rather than conventional diffraction contrast imaging (28–31) was used in this work to understand the characteristics of the dislocations (see *SI Appendix, Fig. S9* and a detailed clarification in *SI Appendix*). Fig. 2*A* and *Movie S2* present time-resolved HRTEM images and schematic illustrations showing the climb dynamics of a dislocation during in situ Li-ion deintercalation. The dislocation motion mainly involves a negative climb. Note that, unlike climbing in a uniform crystal with the same equilibrium lattice constant everywhere, the misfit dislocation climb between inhomogeneously delithiated phases/domains does not require long-range diffusional removal of TM or O vacancies. The departure of Li cation, and the resulting change in TM cation valence and cation radius, would cause transformational strain, and this strain can displace TM ions, which are directly visualized in the TEM. Fig. 2*B* and *Movie S3* present time-resolved HRTEM images and schematic illustrations showing the glide dynamics of a dislocation dipole during in situ Li-ion deintercalation. Statistical analyses were performed to quantitatively understand the dislocation motion kinetics. Fig. 2 *C* and *D* show the measured climb and glide velocities of individual dislocations during electrochemical delithiation under an applied voltage of  $\sim 5$  V. The average dislocation climb and glide velocities are determined to be approximately 0.18 nm/s and 0.38 nm/s, respectively, suggesting that they are of the same order of magnitude.

Atomistic dynamics of versatile dislocation activities were further revealed during in situ Li-ion intercalation. Fig. 3 *A* and *B*

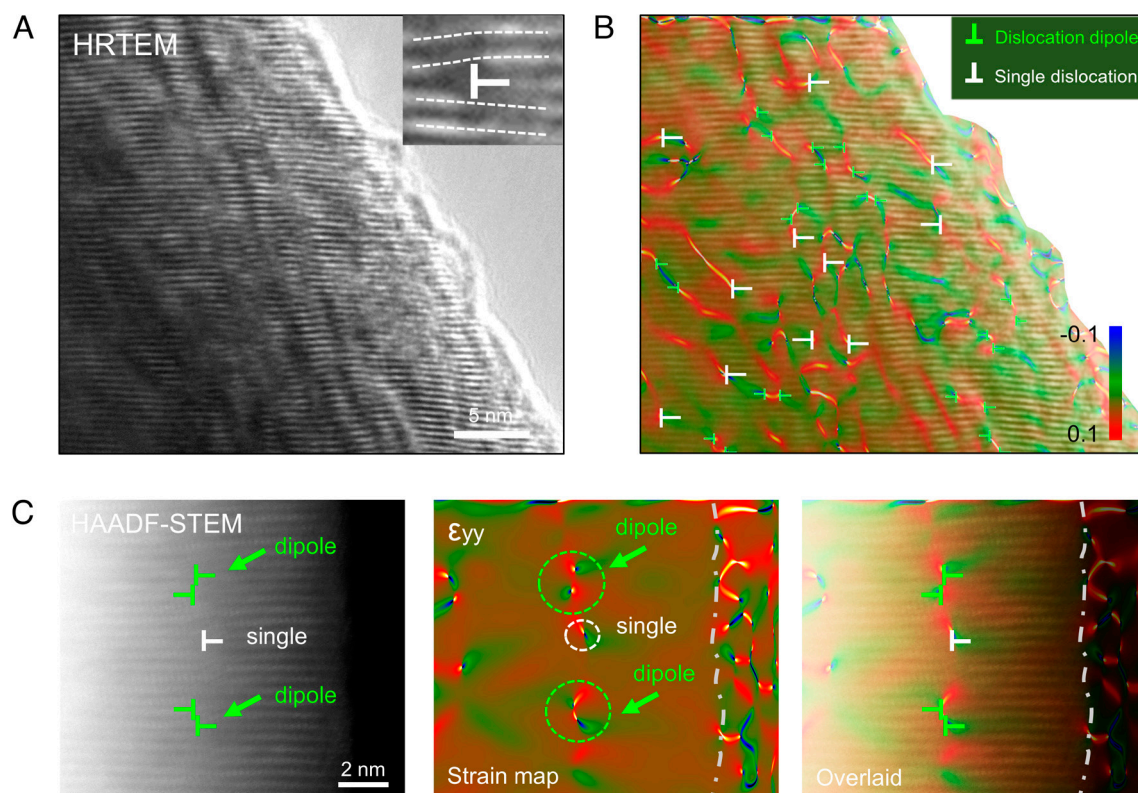


**Fig. 1.** Nonuniform ion-deintercalation-induced misfit dislocations in layered oxides. (A) HRTEM image showing the formation of substantial single dislocations and dislocation dipoles in lithium nickelate after in situ Li-ion deintercalation at  $\sim 5$  V. (B) Strain map corresponding to the HRTEM image in (A). (C) Atomic-resolution HAADF-STEM image (zone axis close to *a* or *b* axis) and corresponding strain maps of lithium nickelate electrochemically charged to 4.4 V in coin cells.

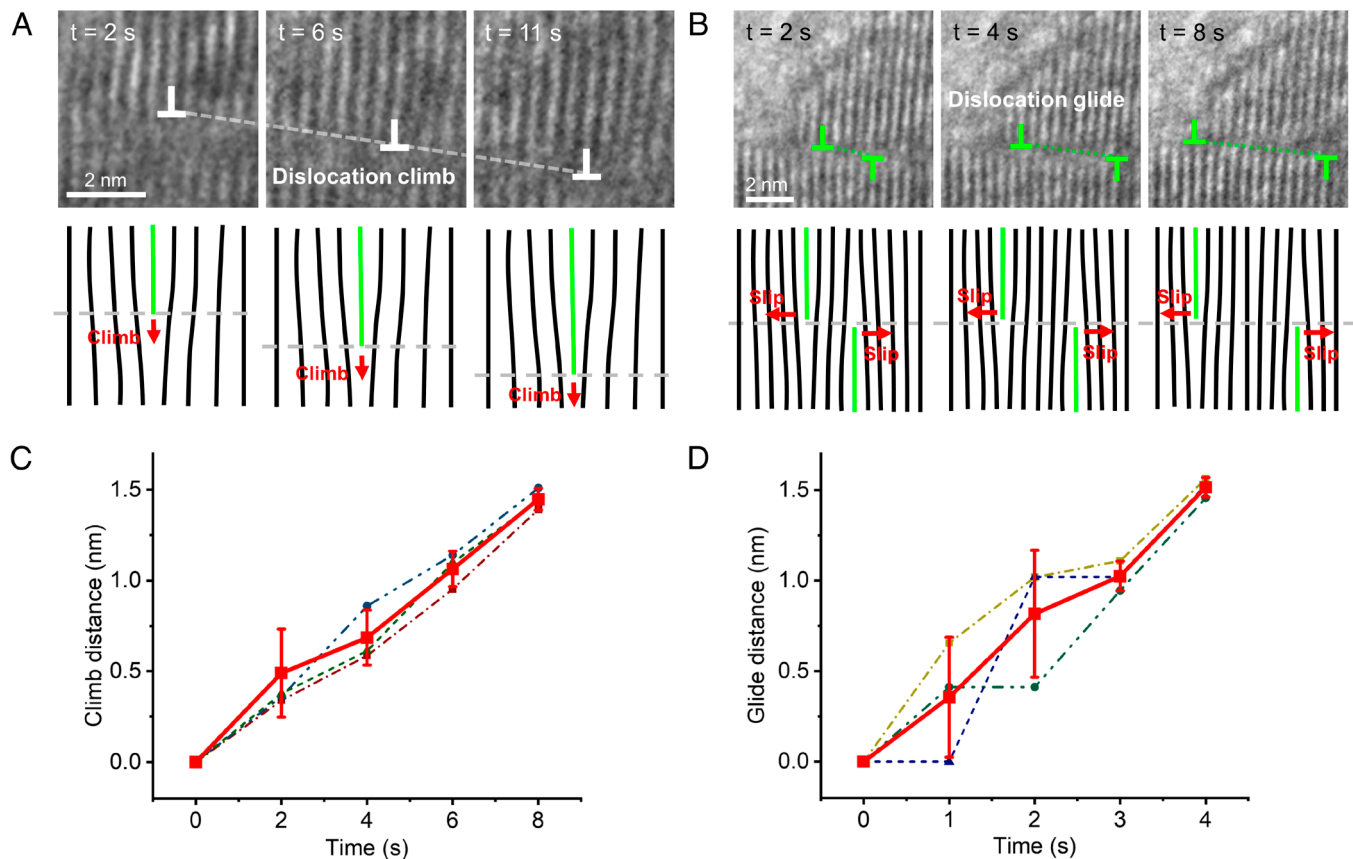


**Fig. 2.** Direct measurement of dislocation glide and climb velocities during electrochemical delithiation. (A) Time-resolved HRTEM images and schematic illustrations showing the climb dynamics of a dislocation. (B) Time-resolved HRTEM images and schematic illustrations showing the glide dynamics of a dislocation dipole. (C and D) Statistical measurement of (C) climb velocity and (D) glide velocity for individual dislocations. The solid lines represent the average climb/glide distance over time, with error bars indicating the SD. The dashed lines (in different colors) represent measurements obtained from three independent dislocations.

and [Movie S4](#) present time-resolved HRTEM images and schematics showing the nucleation and evolution dynamics of a dislocation dipole. The Burgers circuit (without closure failure) shows that the original lattice has a perfect structure ( $t = 1$  s). In a second, a dislocation dipole, i.e., two dislocations (the separation between the dislocation cores is less than 1 nm) of opposite signs simultaneously formed from the lattice. The misfit dislocation dipole soon underwent an expansion ( $t = 2$  s) through pure glide (the spacing between the dislocation cores perpendicular to the slip plane remained constant). Subsequently, the dislocation dipole annihilated ( $t = 15$  s) through reversed dislocation glides. Fig. 3C and [Movie S5](#) show the motion dynamics of two adjacent dislocation dipoles. First, upon delithiation, a dislocation dipole (denoted as dipole1) grew out of the perfect lattice nearly through pure glide ( $t = 10$  s). Subsequently, another dislocation dipole, i.e., dipole2 (right side) formed right next to the preexisting dipole1; meanwhile, dislocation dipole1 remained stable as the spacing between the two component dislocations did not change. Soon, dipole2 expanded through mixed glide and climb, leading to slightly increased spacing between the dislocation cores; meanwhile, dipole1 vanished through reversed glide and annihilation of the component dislocations. Fig. 3D and [Movie S6](#) show the motion dynamics of a single dislocation and a dislocation dipole adjacent to each other. After nucleation, the single dislocation underwent both glide (to the left) and climb (upward) ( $t = 10$  s). After that, a dislocation dipole with a core separation of around 2 nm soon nucleated right next to the single dislocation ( $t = 15$  s). Subsequently, the dipole expanded through pure climb of the upper dislocation, while the lower dislocation in the dipole, as

well as the single dislocation, remained stable ( $t = 17$  s). The observed versatile dislocation motions, including pure glide, pure climb, and mixed motions, indicate that the electrochemically driven dislocation activities in lithium nickelate are quite random and complex, which is caused by inhomogeneous  $\text{Li}^+$  ion deintercalation and transport at the atomic scale, that causes inhomogeneous transformation strains.

To explore the impact of dislocation formation on layered cathode's structural and chemomechanical degradation, we performed statistical atomic-scale imaging of layered oxides electrochemically cycled within real batteries. As shown in Fig. 4A and B, the rock salt (RS) phase—an electrochemically inactive and detrimental phase triggered by concurrent lattice oxygen loss and cation mixing—was found to preferentially nucleate in the form of nanodomains around individual dislocations and dislocation dipoles. Meanwhile, dislocation formation-mediated lattice expansion (indicated by the arrow in Fig. 4C), which has been previously reported to lead to crack embryo nucleation (32), was also observed in  $\text{LiNiO}_2$  during electrochemical operation. These results confirm that dislocations could indeed serve as universal preferential sites for both detrimental phase transformation and mechanical failure in layered oxides. Moreover, we also observed local lattice reorientation induced by intense dislocation nucleation-annihilation (Fig. 5 and [Movie S7](#)). Fig. 5A shows that before Li-ion deintercalation, the pristine layered cathode consists of two domains (domain1 and domain2). While domain2's lattice fringes [with a d-spacing of 0.47 nm corresponds the (003) crystallographic planes of  $\text{LiNiO}_2$ ] are resolved, domain1's lattice is not clearly resolved due to a slight misorientation possibly

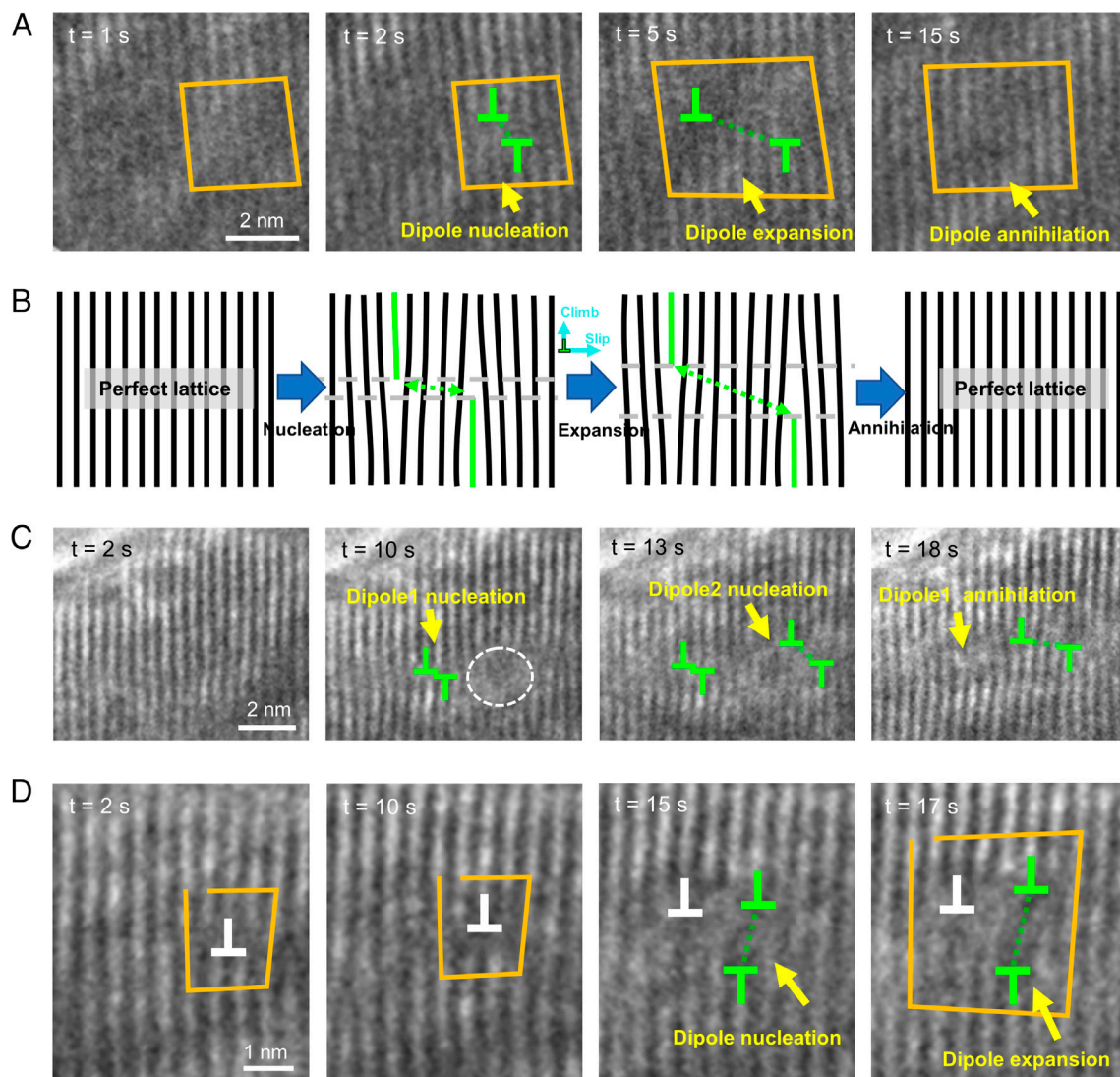


**Fig. 3.** Atomistic dislocation dynamics during in situ Li-ion deintercalation under an applied voltage of 5 V. (A) Time-resolved HRTEM images showing the process of nucleation ( $t = 2$  s), expansion ( $t = 4$  s), and annihilation ( $t = 15$  s) of a dislocation dipole. (B) Schematic illustrations of the dislocation dynamics corresponding to (A). (C) The motion dynamics of two adjacent dislocation dipoles. Upon nucleation, dislocation dipole1 remained stable for a few seconds and soon annihilated; in contrast, dislocation dipole2 underwent expansion with mixed glide and climb motion soon after nucleation. (D) Motion dynamics of adjacent single dislocation and dislocation dipole. The single dislocation underwent both glide and climb motion during the whole process; while the dislocation dipole underwent expansion through pure climb of the upper dislocation.

occasionally introduced during calcination as reported by previous works (33). Upon possibly localized Li-ion deintercalation, a large bunch of dislocations burst out from the domain interface (Fig. 5B). Subsequently, the dislocation densities at the domain

interface decreased rapidly through annihilation of dislocations of opposite signs (Fig. 5 C and D). Ultimately, with the dislocation densities further reduced (Fig. 5 E and F), domain1 reoriented to nearly the same orientation as domain2. This previously

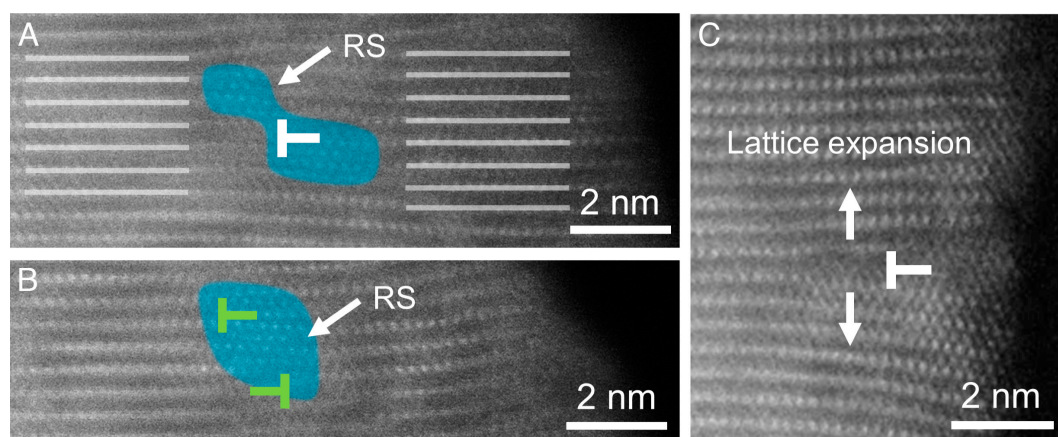


**Fig. 4.** Dislocation formation-mediated structural and mechanical degradation of layered oxides. (A and B) RS phase transformation promoted by (A) individual dislocation and (B) dislocation dipole formation in electrochemically operated layered oxides. The RS nanodomains are highlighted in cyan. (C) Dislocation formation-mediated crack embryo nucleation. The abnormal lattice expansion around the dislocation core is indicated by the arrow.

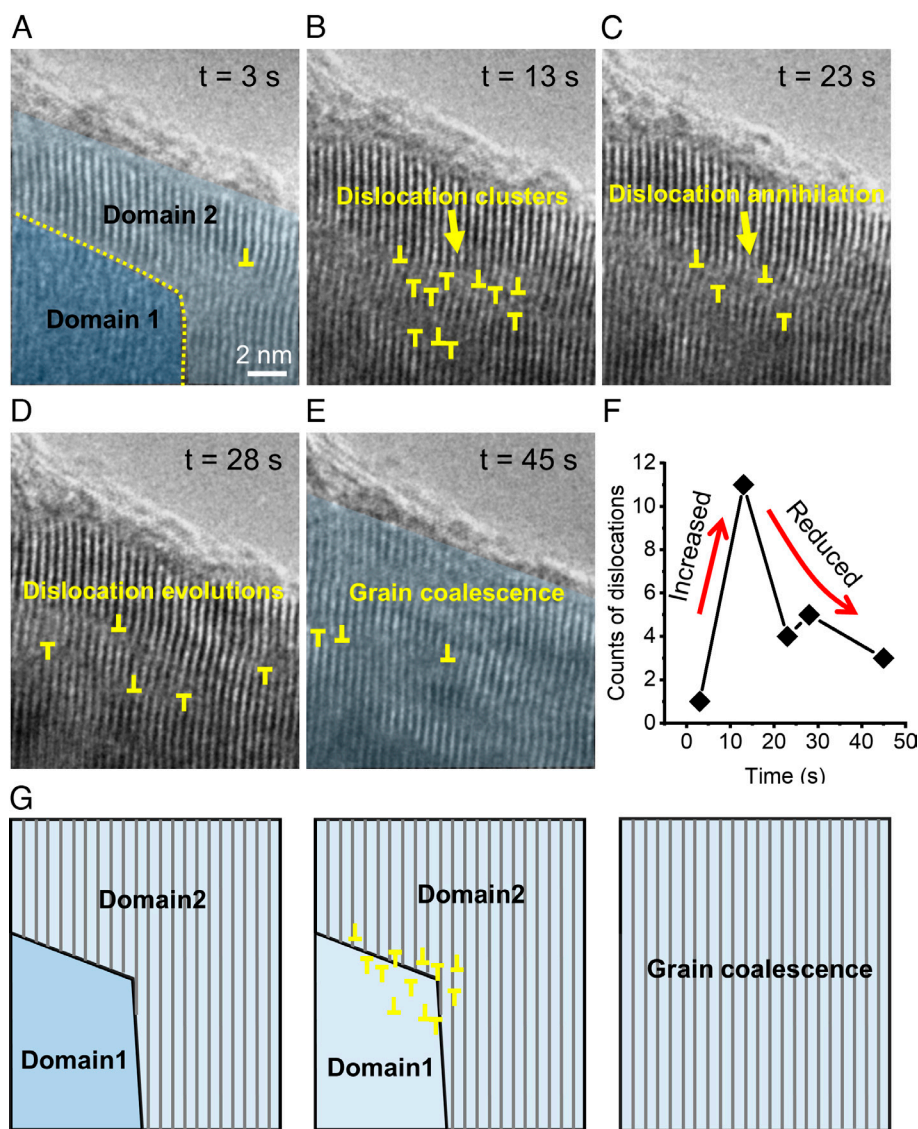


**Fig. 5.** Dislocation burst-annihilation-induced domain reorientation. (A) The initial structure of a lithium nickelate particle composed of two domains. (B) Dislocation burst at the domain interface. (C–E), Coalescence of the two domains through annihilation of dislocations at the domain interface. (F) Counts of the interfacial dislocations as a function of time. (G) Schematic illustration of the dislocation burst-annihilation-mediated lattice reorientation.

unrecognized dislocation burst-annihilation induced domain reorientation, as schematically illustrated in Fig. 5G, could have an important influence on Li-ion transport within layered oxides, warranting further investigation in future studies.

## Discussion

Dislocation movement in ceramics is inherently sluggish when compared to metals (34, 35). This deceleration can be attributed to the strong ionic and covalent bonds that naturally impede dislocation mobility. Generally, depending on variables such as crystal structure, temperature, and other factors, dislocation glide velocities in ceramics tend to fall within the range of  $10^{-12}$  to  $10^{-8}$  m/s, while climb velocities are typically on the order of  $10^{-15}$  to  $10^{-12}$  m/s (36), with the latter being a few orders of magnitude slower. In contrast to conventional expectations, our research, in the context of electrochemical reactions, reveals a noteworthy departure from this norm. Specifically, we found that, in layered oxides, the electrochemically driven dislocation climb exhibits an average velocity ( $\sim 0.38$  nm/s) comparable to that of dislocation glide ( $\sim 0.18$  nm/s). This observation suggests

a significant increase in climb velocity relative to glide velocity, likely originating from the inherent instability of layered oxides, particularly the most unstable pure  $\text{LiNiO}_2$ . Specifically, the enhanced climb velocity can be attributed to two distinct characteristics that distinguish layered oxides from conventional ceramics like structural ceramics: First, the electrochemical deintercalation process generates substantial Li vacancies that provide abundant favorable empty sites for transition metal (TM) ion diffusion, a critical factor in accelerating dislocation climb kinetics. Second, the electrochemically triggered oxygen loss, which is universal in layered oxides, largely debonds TM ions from the TM-O octahedra, thus lowering the energy barrier for dislocation climb through TM ion diffusion.

Oxygen evolution occurs during in situ TEM deintercalation, albeit to a very limited extent. For example, only a small amount of RS phase (indicative of oxygen loss) was identified on the outermost particle surface during in situ deintercalation (Fig. 5). Meanwhile, RS phase or cation mixing was not identified during dislocation nucleation, interaction, and annihilation processes as shown in Figs. 2 and 3. This suggests that oxygen loss had a trivial role in the observed dislocation activities initially. However,

extended electrochemical cycling, as in the case of the long-cycled layered oxides in Fig. 4, led to enhanced oxygen loss, especially around dislocation cores. This indicates that while oxygen evolution may not be a prominent factor in the early stages of dislocation activities, it can be significantly promoted by dislocation activities with prolonged electrochemical cycling.

In conclusion, by performing in situ electron microscopy observations, we deciphered the complex dislocation activities driven by nonuniform ion deintercalation in an archetypal layered oxide cathode for lithium-ion batteries. The nucleation, motion, and annihilation dynamics of misfit dislocations within the inhomogeneously deintercalated lattice were directly captured with atomic resolution. The dislocation glide and climb velocities in layered oxides were experimentally measured. Moreover, dislocation generation-triggered chemomechanical degradation and local lattice reorientation were also uncovered. Our work, by providing direct visualization of the dynamic behaviors of topological defects during electrochemical reactions, offers important insights into the dislocation activity and dislocation-controlled structural degradation of layered oxide cathode materials.

## Materials and Methods

**Sample Preparation.** The lithium nickelate ( $\text{LiNiO}_2$ ) layered oxide was prepared by coprecipitation followed by calcination. For the coprecipitation, a 0.1 M  $\text{NiSO}_4 \cdot 6\text{H}_2\text{O}$  solution was pumped into  $\text{NaOH}$  and  $\text{NH}_3 \cdot \text{H}_2\text{O}$  aqueous solution (the molar ratio of  $\text{NaOH}/\text{NH}_3$  is 1.2) under the protection of  $\text{N}_2$  at 55 °C. The prepared hydroxide precipitates were washed with deionized water, collected,

and dried in a vacuum oven at a temperature of 105 °C or 12 h. The coprecipitated hydroxide precursors were mixed with  $\text{LiOH}$  powders, calcined at 460 °C for 2 h, and then 700 °C for 6 h under oxygen flow to obtain the  $\text{LiNiO}_2$  layered oxides.

**In Situ TEM Experiments.** In situ TEM experiments were conducted with a scanning tunneling microscopy-TEM system in a transmission electron microscope (equipped with an X-FEG field emission source) operated under 200 KV. The in situ delithiation experiments were performed by applying a bias between a Cu substrate and a piezo-controlled W probe ( $\text{LiNiO}_2$  layered ceramic particles were inserted between the Cu substrate and the W probe). By scratching a small amount of lithium metal with the W probe and exposing it to air for seconds, a surface passivation layer mainly composed of lithium oxide was intentionally formed to act as a Li-ion conductor to enable the delithiation of  $\text{LiNiO}_2$ .

**Data, Materials, and Software Availability.** All study data are included in the article and/or supporting information.

**ACKNOWLEDGMENTS.** This work is supported by the Materials Science and Engineering Divisions, Office of Basic Energy Sciences of the U.S. Department of Energy, under award no. DE-SC0021204. J.L. acknowledges support by NSF CBET-2034902. This research used resources of the Center for Functional Nanomaterials, which is a U.S. Department of Energy Office of Science User Facility, at Brookhaven National Laboratory under Contract No. DE-SC0012704.

Author affiliations: <sup>a</sup>Department of Physics and Astronomy, University of California, Irvine, CA 92697; <sup>b</sup>Shenyang National Laboratory for Materials Science, Institute of Metal Research, Chinese Academy of Sciences, Shenyang 110016, China; <sup>c</sup>Department of Nuclear Science and Engineering, Massachusetts Institute of Technology, Cambridge, MA 02139; and <sup>d</sup>Department of Materials Science and Engineering, Massachusetts Institute of Technology, Cambridge, MA 02139

1. D. Hull, D. J. Bacon, *Introduction to Dislocations* (Butterworth-Heinemann, Boston, ed. 4, 2001), p. 242, p. vii.
2. B.-Y. Liu *et al.*, Large plasticity in magnesium mediated by pyramidal dislocations. *Science* **365**, 73–75 (2019).
3. H. Zheng *et al.*, Discrete plasticity in sub-10-nm-sized gold crystals. *Nat. Commun.* **1**, 144 (2010).
4. C. Wang *et al.*, Size-dependent grain-boundary structure with improved conductive and mechanical stabilities in sub-10-nm gold crystals. *Phys. Rev. Lett.* **120**, 186102 (2018).
5. T. E. Mitchell, K. P. D. Lagerlöf, A. H. Heuer, Dislocations in ceramics. *Mater. Sci. Technol.* **1**, 944–949 (2013).
6. S. Wiederhorn, Brittle fracture and toughening mechanisms in ceramics. *Annu. Rev. Mater. Sci.* **14**, 373–403 (1984).
7. M. W. Chen, J. W. McCauley, D. P. Dandekar, N. K. Bourne, Dynamic plasticity and failure of high-purity alumina under shock loading. *Nat. Mater.* **5**, 614–618 (2006).
8. A. Ulvestad *et al.*, Topological defect dynamics in operando battery nanoparticles. *Science* **348**, 1344–1347 (2015).
9. S. Ahmed *et al.*, Understanding the formation of antiphase boundaries in layered oxide cathode materials and their evolution upon electrochemical cycling. *Matter* **4**, 3953–3966 (2021).
10. Q. Li *et al.*, Dynamic imaging of crystalline defects in lithium-manganese oxide electrodes during electrochemical activation to high voltage. *Nat. Commun.* **10**, 1692 (2019).
11. R. Zhang *et al.*, Compositionally complex doping for zero-strain zero-cobalt layered cathodes. *Nature* **610**, 67–73 (2022).
12. R. Zhang *et al.*, Long-life lithium-ion batteries realized by low-Ni, Co-free cathode chemistry. *Nat. Energy* **8**, 695–702 (2023).
13. Y. Bi *et al.*, Reversible planar gliding and microcracking in a single-crystalline Ni-rich cathode. *Science* **370**, 1313–1317 (2020).
14. J. Li *et al.*, Dynamics of particle network in composite battery cathodes. *Science* **376**, 517–521 (2022).
15. W. Li, E. M. Erickson, A. Manthiram, High-nickel layered oxide cathodes for lithium-based automotive batteries. *Nat. Energy* **5**, 26–34 (2020).
16. T. Liu *et al.*, Understanding Co roles towards developing Co-free Ni-rich cathodes for rechargeable batteries. *Nat. Energy* **6**, 277–286 (2021).
17. P. Yan *et al.*, Injection of oxygen vacancies in the bulk lattice of layered cathodes. *Nat. Nanotechnol.* **14**, 602–608 (2019).
18. T. Zhou *et al.*, Stabilizing lattice oxygen in slightly Li-enriched nickel oxide cathodes toward high-energy batteries. *Chem* **8**, 2817–2830 (2022).
19. C. Wang *et al.*, Resolving atomic-scale phase transformation and oxygen loss mechanism in ultrahigh-nickel layered cathodes for cobalt-free lithium-ion batteries. *Matter* **4**, 2013–2026 (2021).
20. H.-H. Ryu, K.-J. Park, C. S. Yoon, Y.-K. Sun, Capacity fading of Ni-rich  $\text{Li}[\text{Ni}_x\text{Co}_y\text{Mn}_{1-x-y}]\text{O}_2$  ( $0.6 \leq x \leq 0.95$ ) cathodes for high-energy-density lithium-ion batteries: Bulk or surface degradation? *Chem. Mater.* **30**, 1155–1163 (2018).
21. C. S. Yoon, D.-W. Jun, S.-T. Myung, Y.-K. Sun, Structural stability of  $\text{LiNiO}_2$  cycled above 4.2 V. *ACS Energy Lett.* **2**, 1150–1155 (2017).
22. C. Wang *et al.*, Resolving complex intralayer transition motifs in high-Ni-content layered cathode materials for lithium-ion batteries. *Nat. Mater.* **22**, 235–241 (2023).
23. C. Wang *et al.*, Direct observation of chemomechanical stress-induced phase transformation in high-Ni layered cathodes for lithium-ion batteries. *Matter* **6**, 1265–1277 (2023).
24. C. Wang, R. Zhang, K. Kisslinger, H. L. Xin, Atomic-scale observation of O1 faulted phase-induced deactivation of  $\text{LiNiO}_2$  at high voltage. *Nano Lett.* **21**, 3657–3663 (2021).
25. F. Xia *et al.*, Revealing structural degradation in layered structure oxides cathode of lithium ion batteries via in-situ transmission electron microscopy. *J. Mater. Sci. Technol.* **154**, 189–201 (2023).
26. X. H. Liu *et al.*, In situ TEM experiments of electrochemical lithiation and delithiation of individual nanostructures. *Adv. Energy Mater.* **2**, 722–741 (2012).
27. R. Sinclair, In situ high-resolution transmission electron microscopy of material reactions. *MRS Bull.* **38**, 1065–1071 (2013).
28. J. M. Zuo, J. C. Spence, *Advanced Transmission Electron Microscopy* (Springer, 2017).
29. C. L. Jia, A. Thust, K. Urban, Atomic-scale analysis of the oxygen configuration at a  $\text{SrTiO}_3$  dislocation core. *Phys. Rev. Lett.* **95**, 225506 (2005).
30. H. Gabrisch, R. Yazami, B. Fultz, The character of dislocations in  $\text{LiCoO}_2$ . *Electrochem. Solid-State Lett.* **5**, A111–A114 (2002).
31. T. J. Balk, K. J. Hemker, High resolution transmission electron microscopy of dislocation core dissociations in gold and iridium. *Philos. Mag. A* **81**, 1507–1531 (2001).
32. P. Yan *et al.*, Intragranular cracking as a critical barrier for high-voltage usage of layer-structured cathode for lithium-ion batteries. *Nat. Commun.* **8**, 14101 (2017).
33. S. Y. Lee *et al.*, Revisiting primary particles in layered lithium transition-metal oxides and their impact on structural degradation. *Adv. Sci.* **6**, 1800843 (2019).
34. J. Wang, R. G. Hoagland, A. Misra, Room-temperature dislocation climb in metallic interfaces. *Appl. Phys. Lett.* **94**, 134 (2009).
35. W. F. Greenman, T. Vreeland, D. S. Wood, Dislocation mobility in copper. *J. Appl. Phys.* **38**, 3595–3603 (1967).
36. B. Y. Farber, A. S. Chiarelli, A. H. Heuer, Dislocation velocities in cubic zirconia ( $\text{ZrO}_2$ ) single crystals. *Philos. Mag. A* **72**, 59–80 (1995).